

Chiral superconductivity in the doped triangular-lattice Fermi-Hubbard model in two dimensions

Vinicius Zampronio^{1,2} and Tommaso Macrì^{3,2}

¹Institute for Theoretical Physics, Utrecht University, 3584CS Utrecht, Netherlands

²Departamento de Física Teórica e Experimental, Federal University of Rio Grande do Norte 59078-950 Natal-RN, Brazil

³ITAMP, Harvard-Smithsonian Center for Astrophysics, Cambridge, Massachusetts 02138, USA

The triangular-lattice Fermi-Hubbard model has been extensively investigated in the literature due to its connection to chiral spin states and unconventional superconductivity. Previous simulations of the ground state of the doped system rely on quasi-one-dimensional lattices where true long-range order is forbidden. Here we simulate a 12×12 triangular lattice using state-of-the-art Auxiliary-Field Quantum Monte Carlo. Upon doping a non-magnetic chiral spin state, we observe evidence of chiral superconductivity at filling $n = 5/6$ supported by long-range order in Cooper-pair correlation and a finite value of the chiral order parameter. With this aim, we first locate the transition from the metallic to the non-magnetic insulating phase where we see competition between chiral and magnetic orders. Our results pave the way towards a better understanding of strongly correlated lattice systems with magnetic frustration.

As one of the key paradigms of strongly correlated fermionic lattice systems, the Fermi-Hubbard (FH) model still has many open questions [1]. In two dimensions (2D), the FH captures the rich physics of metal to insulator phase transitions (MIT) [2], itinerant magnetism [3] and spin liquids [4, 5, 6]. Quantum spin liquids with non-abelian anyon excitations can act as building blocks for topological quantum computation and to the construction of fault-tolerant quantum computers [7]. The idea behind this non-magnetic insulator was proposed in the seminal work by Anderson that describes a resonating valence-bond state arising from geometric frustration on the lattice [8, 9]. The simplest lattice structure containing this kind of frustration is the triangular one, which is relevant for the un-

derstanding of molecular materials of the κ -ET family [10, 11, 12, 13, 14]. Besides geometrical frustration, charge fluctuations play a role in the stabilization of quantum spin liquids [15, 16]. The simulation of charge fluctuations can be accomplished by introducing high-order ring-exchange coupling to the effective spin Hamiltonian [17, 18, 19, 20] or by considering the Hubbard model itself. Additionally, the observation of Hubbard-model physics in triangular lattices engineered in $\text{WeSe}_2/\text{WeS}_2$ moiré superlattices [21, 22] and in quantum simulators [23] arouses scientific interest in such systems. In this work, we focus on the triangular-lattice FH model described by the Hamiltonian

$$H = -t \sum_{\langle ij \rangle, \alpha} (c_{i\alpha}^\dagger c_{j\alpha} + \text{H.c.}) + U \sum_i n_{i\uparrow} n_{i\downarrow}, \quad (1)$$

where $\alpha = \uparrow, \downarrow$ is the electron spin, $\langle ij \rangle$ indicates a sum over nearest neighbours sites, $c_{i\alpha}$ and $c_{i\alpha}^\dagger$ respectively annihilates and creates an electron with spin α at the i -th lattice site, $n_{i\alpha} = c_{i\alpha}^\dagger c_{i\alpha}$ is the number operator, t is the hopping strength and U is the intensity of the onsite interaction. The non-interacting system is metallic and, at half-filling ($\langle n_{i\alpha} \rangle = 1/2$), the strongly interacting FH Hamiltonian can be mapped into the antiferromagnetic (AFM) Heisenberg one, whose ground state contains 120° long-range spin order [24]. Away from this two cases ($U/t = 0$ and $U/t \gg 1$) the precise nature of the system is still under debate. For weak interactions, numerical simulations assume an adiabatic connection with the non-interacting regime. Nonetheless, they might be overlooking a transition to a phase with a small but non-vanishing gap [1]. In fact, renormalization-group calculations predict a $d + id$ superconductor at $U/t \ll 1$ in 2D [25, 26] and weak coupling analyses argue that at weak interactions the quasi-1D system is a Luther-Emery

liquid with time-reversal symmetry breaking [27]. For intermediate interactions much interest is devoted to the quest for a chiral spin liquid (CSL) due to its relation to the quantum Hall effect and time-reversal symmetry breaking [28, 29, 30]. Still, there is not even theoretical agreement on whether the spin liquid state exists in the FH model. While calculations ranging from variational cluster approximation [31, 32, 33], path integral renormalization group [34, 35], strong coupling expansion [19], dual fermion approach [36] and exact diagonalization [37] to density matrix renormalization group (DMRG) [38, 39, 40, 41] and variational Monte Carlo (VMC) [42, 43] agreed in the existence of a spin liquid state, dynamical cluster approximation studies [44] and earlier VMC computations [45, 46] detected a direct transition from a metallic state to a magnetic ordered phase. Among the theories that support the existence of a spin liquid, infinite-DMRG calculations predict a gapped CSL [39, 40], while VMC simulations on full 2D systems and finite-DMRG [38] support a gapless spin liquid that preserves time-reversal symmetry. On the other hand, a multi-method approach finds that, at intermediate interactions, there is a competition between chiral and two distinct magnetic orders: collinear and 120° order [47]. For the hole-doped system, the quest for unconventional superconductivity in the Hubbard model is a matter of current scientific interest due to its connection to High- T_c superconductors [48, 49, 50, 51]. A recent DMRG study of the doped triangular FH predicts a rich phase diagram with fractionalized excitations, spin and charge deconfinement and enhanced Cooper-pair correlations [52]. Spin and charge deconfinement in this system has also been observed experimentally [53]. Another DMRG study estimates the spectral function of one single hole doped in the triangular-lattice CSL and observes spinon dynamics [54]. Also, DMRG simulations of the extended $t - J$ model in the triangular lattice indicate the emergence of a chiral superconductor, evidenced by quasi-long-range-order in the Cooper-pair correlations upon doping [55]. However, DMRG performed in quasi-1D lattices does not display true long-range order, and one has to rely on a slow decay of Cooper-pair correlations. Numerical simulations via the Linked-Cluster Expansion algorithm provide several benchmarks to the finite temperature

triangular FH at intermediate to strong interactions [56], but a clear description of the weakly interacting regime, the classification of the spin liquid state, and whether or not a superconducting phase would appear upon doping is still elusive.

In this work, we investigate the ground state of the doped triangular FH in 2D employing *ab initio* numerical techniques. Upon doping a non-magnetic chiral spin state (CSS) we observe true long-range order in the Cooper-pair correlations while the chiral order parameter remains finite, i.e. a chiral superconductor. To simulate the CSS, we first locate the MIT and investigate chiral and magnetic orders in the insulating phase.

1 Methods

We report the implementation of state-of-the-art Auxiliary-Field Quantum Monte Carlo (AFQMC) to simulate the ground state of the full 2D triangular lattice FH model. By imaginary-time projection to the ground state we intend to reduce the bias from VMC calculations. A constrained-path approximation is required to restore polynomial convergence (otherwise plagued by the sign problem [57]) and the bias from the variational ansatz is not completely removed. However, simulations made in the past for square lattices away from half-filling showed to be accurate and provided several benchmarks [58, 59, 60, 61, 62]. See the Appendix A for further details of the method.

The *ansatz* we choose for the imaginary-time projection is a generalized Hartree-Fock (GHF) trial state. The mean-field Hamiltonian associated to the GHF state is obtained considering a partial particle-hole transformation on a BCS Hamiltonian,

$$H_{\text{MF}} = -t \sum_{\langle ij \rangle \alpha} c_{i\alpha}^\dagger c_{j\alpha} + \sum_i M_i c_{i\uparrow}^\dagger c_{i\downarrow} + \text{H.c.}, \quad (2)$$

where $M_i = U_{\text{eff}} \langle c_{i\uparrow}^\dagger c_{i\downarrow} \rangle$. The GHF ground state is obtained via a self-consistent diagonalization of Eq. (2) [62]. As done with Unrestricted Hartree Fock (UHF) wave functions [61], we consider $U_{\text{eff}} = \min(U, 4t)$. A noticeable advantage of GHF states over UHF ones in triangular lattices is the possibility of the former to capture spin textures in the xy -plane which are expected to hold in the strong interaction regime. We noticed

that the constrained-path AFQMC becomes unstable for strong interactions. For that reason we restrict our simulations to interactions $U/t \leq 12$. In this regime of interactions we were able to capture the transition to the non-magnetic insulating phase.

In our simulations, the largest lattice we consider has periodic boundary conditions (PBC) with $N_x = N_y = 12$ sites along the $\hat{e}_x = (a, 0)$ and $\hat{e}_y = (a/2, \sqrt{3}a/2)$ directions respectively (see FIG. 1 for the lattice vectors and a visual representation of the triangular FH model). We also run simulations with smaller lattices with $N_x = 9$ and $N_y = 12$ to analyse the finite-size effects. See the Appendix B for the dependence of total energy on the lattice size. Finally, to address the effect of the dimensionality, we investigate quasi-1D lattices with $N_x = 36$, $N_y = 3$, PBC along \hat{e}_y and open boundary condition along \hat{e}_x . From now on, if not specified otherwise, we are considering the 12×12 lattice. We study spin-balanced systems at half filling ($n = N/M = 1$, where N is the number of electrons and $M = N_x N_y$) and with hole doping ($n < 1$).

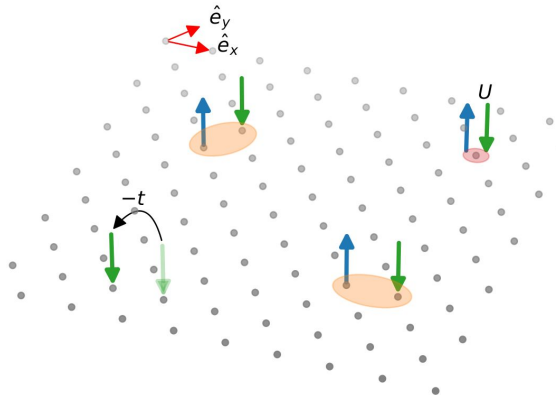


Figure 1: **Triangular FH model.** We display the lattice vectors $\hat{e}_x = (a, 0)$ and $\hat{e}_y = (a/2, \sqrt{3}a/2)$. The circle depicts the formation of a doublon (doubly-occupied site) with energy cost U . We also represent a hopping process and the $-t$ energy decrease. Ellipses depict Cooper pairs in the singlet ($|s\rangle = (|\uparrow\rangle - |\downarrow\rangle)/\sqrt{2}$) or triplet ($|t\rangle = (|\uparrow\rangle + |\downarrow\rangle)/\sqrt{2}$) states formed on the \hat{e}_x and \hat{e}_y bounds of the triangular plaquettes.

2 Results at half filling

We start by defining the charge structure factor

$$N(\mathbf{k}) = \frac{1}{M} \sum_{i,j} e^{\mathbf{k} \cdot \mathbf{r}_{ij}} (\langle n_i n_j \rangle - \langle n_i \rangle \langle n_j \rangle), \quad (3)$$

with $n_i = n_{i\uparrow} + n_{i\downarrow}$, around the origin $\mathbf{k} = 0$ to determine whether the system is gapped or not. Since the charge gap $\Delta_c \propto \lim_{k \rightarrow 0} k^2/N(k)$ [63, 64], a linear behavior around $k = 0$ indicates that the system is metallic (gapless) and a quadratic behavior indicates that the system is insulating (gapped). More precisely, for small k we have $N(k) = ak^2 + bk + \mathcal{O}(k^3)$, and whenever $b \neq 0$, $\Delta_c = 0$. We compute the coefficients a and b by performing a quadratic fit to our data. We considered the three allowed momenta closer to the origin along $\mathbf{k} = (k_x = 0, k_y)$, results are shown in FIG. 2 where we located the MIT around $7 < U_c/t \leq 8$. Our critical interaction is in agreement with DMRG simulations [38, 39] and a multi-method study [47]. The Linked-Cluster-Expansion calculations, after an extrapolation to zero-temperature regime, predict a critical interaction $U_c/t \sim 7$ [56], while another DMRG simulations predict $U_c/t \sim 9$ [41].

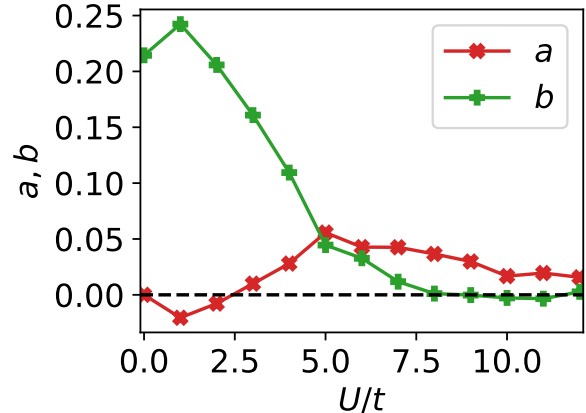


Figure 2: **Metal-insulator transition.** The coefficients of the expansion $N(k) \approx ak^2 + bk$ as a function of the interaction U/t . A nonzero value of b implies that $\Delta_c = 0$.

To further corroborate our findings, we compute the doublon density, $d = \sum_i \langle n_{i\uparrow} n_{i\downarrow} \rangle / M$, for which we expect different behaviors in the metallic and insulating phases [65, 38]. In the metallic phase the Brinkman-Rice picture predicts that d decreases linearly with U [66], while for strong interactions the doublon density shows Heisenberg

behavior [67], $d = (2t^2/U^2 \sum_{\delta} (1/4 - \langle \mathbf{S}_i \cdot \mathbf{S}_{i+\delta} \rangle)$, where the sum runs over the nearest neighbours. In Fig. 3 we display results for d as a function of U/t . Our data for the doublon density show a deviation from the linear behavior near the MIT.

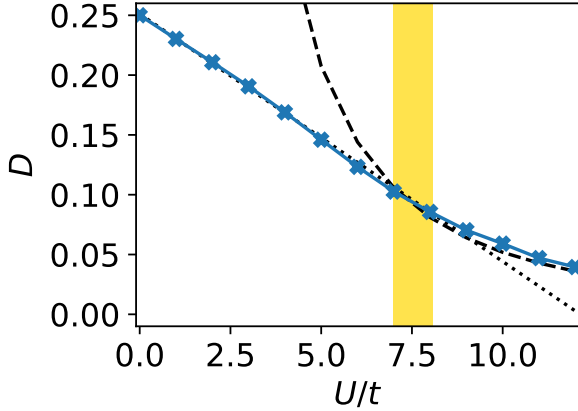


Figure 3: **Doublon density** ('x') as function of the interaction strength U/t . The dotted line is a linear fit of the doublon-density data for $U/t < 7$. The shaded area delimits the region where U_c is in. The dashed curve is the function $d = (2t^2/U^2 \sum_{\delta} (1/4 - \langle \mathbf{S}_i \cdot \mathbf{S}_{i+\delta} \rangle))$ with $\langle \mathbf{S}_i \cdot \mathbf{S}_{i+\delta} \rangle = -0.182$, see Ref. [68]. Error bars are smaller than the markers size.

Analogously, the presence of a spin gap can be accessed by the spin structure factor

$$S(\mathbf{k}) = \frac{1}{M} \sum_{i,j} e^{i\mathbf{k} \cdot \mathbf{r}_{ij}} \langle S_i^z S_j^z \rangle, \quad (4)$$

with $S_i^z = n_{i\uparrow} - n_{i\downarrow}$. $S(k)$ has linear behavior up to $U/t = 11$ (Fig. 4), which indicates the absence of a spin gap and absence of AFM order. Interestingly, for $U/t = 12$, $S(k)$ has a finite value at the origin and a quadratic behavior. The latter is an indication of a spin gap and AFM order. The finite value of $S(k)$ at $k = 0$ is intensified in the smaller (9×12) lattice but occurs at a different interaction. Also, $S(0)$ is always zero for the interactions we have considered in quasi-1D (see Appendix C). We do not exclude the possibility of this being a finite-size effect.

The presence of peaks in $S(k)$ is a signature of long-range magnetic order; for the 120° AFM those peaks appear on the K points of the Brillouin zone. In our simulations we see that the maxima of $S(k)$ form around $k = K$ but no clear formation of peaks (see Appendix C).

We investigate the chiral order parameter

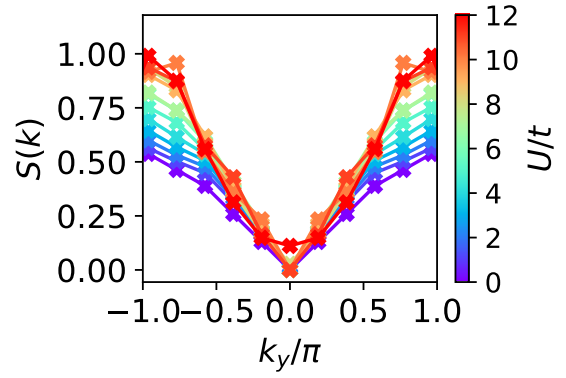


Figure 4: **Spin structure factor** $S(k)$ as a function of U/t for $\mathbf{k} = (k_x = 0, k_y)$. The linear behavior around $k_y = 0$ indicates gapless spin excitation.

$$\chi = \left| \sum_{\triangle} \langle \mathbf{S}_i \cdot (\mathbf{S}_j \times \mathbf{S}_k) \rangle \right|, \quad (5)$$

where the sum is over every triangular plaquette of the lattice with vertexes i, j and k taken in the clockwise direction and $\mathbf{S}_{\ell} = \sum_{\alpha, \beta=\uparrow, \downarrow} c_{\ell\alpha}^{\dagger} \sigma_{\alpha\beta} c_{\ell\beta}$, with $\sigma = (\sigma^x, \sigma^y, \sigma^z)$ a vector of Pauli matrices.

Our results for χ are show in Fig. 5 alongside the S_{\max} of $S(k)$. We observe a competition between chiral and magnetic orders as the interaction increases as reported for quasi-1D lattices [47]. We only see a sharp increase in S_{\max} in the MIT, which is not followed by a spin gap. Our only evidence of AFM order is the quadratic behavior of $S(k)$ for $U/t = 12$ and small k . To analyze the effect of dimension in our results, we compute $S(k)$ and χ for the quasi-1D 36×3 lattice. We see that the results in 2D and quasi-1D agree reasonably well, but in quasi-1D we clearly see the AFM insulator with peaks in $k = M$ (see Appendix C), which is a signature of collinear AFM order. The existence of a CSS was predicted in the non-magnetic insulating phase by DMRG [39, 41, 52]. Surprisingly, we also detect finite chiral order before the transition to the insulating phase ($U/t \leq 7$).

3 Doping the non-magnetic CSS

We search for signals of superconductivity in the doped system by looking at the long-range behavior of Cooper-pair correlations. Following the procedure depicted in Ref. [52] we define the cor-

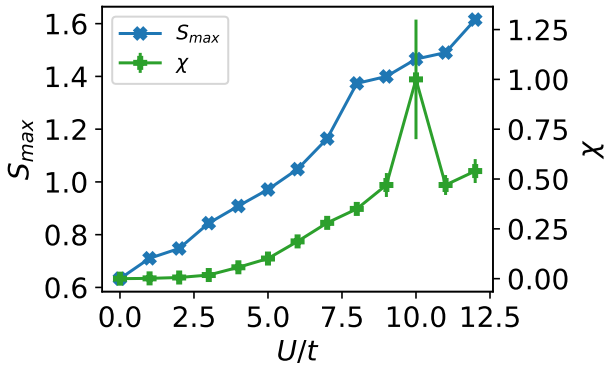


Figure 5: **Magnetic versus chiral orders.** Maximum value of $S(k)$ ('x'). Chiral order parameter χ ('+'). The chiral parameter vertical axis is on the right.

relation function

$$C(\mathbf{r}) = \frac{1}{3M} \sum_{i,\hat{\delta}} \left| \langle \Delta_{i,\hat{\delta}}^\dagger \Delta_{i+\mathbf{r},\hat{\delta}} \rangle \right|, \quad (6)$$

where $\hat{\delta} = \{\hat{e}_x, \hat{e}_y, \hat{e}_x - \hat{e}_y\}$. The superconductivity order parameter $\Delta_{\ell,\hat{\delta}} = (1/\sqrt{2}) \sum_{\alpha} f(\alpha) c_{\ell\alpha} c_{\ell+\hat{\delta}\bar{\alpha}}$, where $\alpha = \uparrow, \downarrow$ and $\bar{\alpha}$ is the opposite spin of α . For pairs in the singlet state $f(\uparrow) = -f(\downarrow) = 1$, and for triplets $f(\uparrow) = f(\downarrow) = 1$. We compute angle-averaged $C(r)$ in the non-magnetic CSS ($U/t = 9$) for three distinct fillings of the hole doped system, $n = 17/18$, $5/6$ and $11/18$, covering the weak-, intermediate- and strong-doping regimes [52]. The results are shown in Fig. 6. Quasi-long-range-order observed in previous DMRG calculations was a hint to the existence of a superconducting phase in the 2D system [52, 55]. Our simulations provide, for the first time, clear evidence of *true* long-range order in the 2D triangular FH model. Furthermore, such long-range correlations increase with the hole concentration. A striking observation is that the chiral order parameter, although reduced, remains finite at the intermediate hole density ($n = 5/6$), $\chi = 0.22(1)$. At the highest hole concentration, the chiral order is further suppressed. At $n = 5/6$, the triplet correlations at large distances are slightly stronger than the singlet ones. Upon further doping the 2D system, the singlet and triplet correlations are (almost) degenerate.

We considered the effect of reduced dimensionality by computing the Cooper-pair correlations in our 36×3 lattice. As expected, we do

not see long-range order in quasi-1D. Still, in the quasi-1D simulations, the triplet and singlet correlations showed to be degenerate (see Appendix C). Notably, recent DMRG simulations showed a strong finite-size dependence. Indeed, singlet-pair correlations dominate for small system sizes, whereas triplet-pair correlations are enhanced for wider cylinders [52].

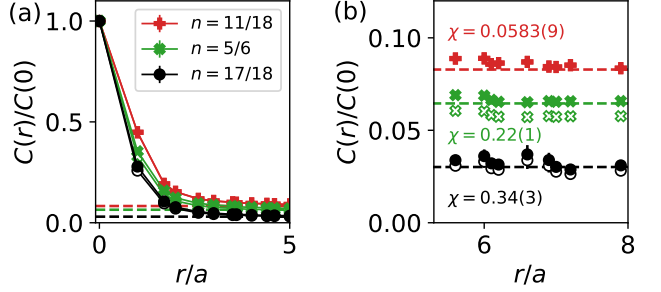


Figure 6: **Cooper pair correlations.** (a) Filled (empty) markers represent correlations between pairs in the triplet (singlet) state. Dashed lines represent an average of the correlations for $r/a \gtrsim 5$ (colors are matching). (b) Long-range behavior of the correlations, the chiral order parameter χ of each system is shown (colors are matching). The interaction strength is $U/t = 9$. When not shown, error bars are smaller than the markers size.

4 Discussion and Conclusion.

We implemented for the first time AFQMC simulations of the zero-temperature triangular-lattice FH model. The method of choice is an *ab initio* technique that provides unbiased estimates subjected to a small systematic error arising from constraints that eliminate the fermionic sign problem. We located the transition to the insulating phase with a critical interaction between $7 < U_c/t \leq 8$ and the presence of a spin gap for $U/t = 12$. We observe a finite value of the chiral order parameter in the three phases observed, and in the insulating phase there is competition between chiral and magnetic orders. Finally, we considered hole doping the non-magnetic CSS near the phase transition at $U/t = 9$. Our results show long-range order in the Cooper-pair correlations.

Topological states that breaks time-reversal symmetry and have quasi-long-range order in the Cooper-pair correlations were observed in DMRG simulations of the $t - J$ model extended to in-

clude tri-spin chiral interactions [55]. Here we reported the simulation of a chiral superconductor in the 2D triangular Hubbard model. For filling $n = 5/6$, we see a finite superconducting order parameter with chiral order and enhanced triplet-pair correlations.

A natural followup of this work would include: (i) The characterization of our CSS via spin-flux insertion to compute the Chern number [39, 55]; (ii) The evaluation of nonlocal correlations to uncover string patterns [69]; (iii) The investigation of quasi-periodic lattices [70, 71] where the interplay between aperiodicity and long-range order leads to exotic phases, analogously to supersolidity [72] and glass physics [73, 74] in Bose systems; (iv) The study of the extended FH model. Long-range interactions can be engineered via Rydberg dressing [75, 76, 77], as recently realised in square lattices with unidirectional hopping [78].

Acknowledgments

We acknowledge Peter Schauss, Davis Garwood, Natanael Costa, Bruno R. de Abreu, Silvio A. S. Vitiello and Federico Becca for insightful discussions. This research was supported by High Performance Computing Center at UFRN (NPAD/UFRN) and Centro Nacional de Processamento de Alto Desempenho em São Paulo (CENAPAD-SP) where the simulations where performed. The software CPMC-Lab [60] was used as an initial guide. V. Z. acknowledges financial support from the Brazilian agencies Coordenação de Aperfeiçoamento de Pesquisa de Pessoal de Nível Superior (CAPES) under the Netherlands Universities Foundation for International Cooperation (NUFFIC) exchange program (process number 88887.649143/2021-00) and the Serrapilheira Institute (grant number Serra-1812-27802). T. M. acknowledges ITAMP for hospitality, where part of this work was done. The source code that was written to generate this results is available in the Quantech simulations repository [79].

References

[1] Daniel P. Arovas et al. “The Hubbard Model”. In: *Annual Review of Condensed Matter Physics* 13.1 (Mar. 2022), pp. 239–274. DOI: [10.1146/annurev-conmatphys-031620-102024](https://doi.org/10.1146/annurev-conmatphys-031620-102024). URL: <https://doi.org/10.1146/annurev-conmatphys-031620-102024>.

[2] Masatoshi Imada, Atsushi Fujimori, and Yoshinori Tokura. “Metal-insulator transitions”. In: *Rev. Mod. Phys.* 70 (4 1998), pp. 1039–1263. DOI: [10.1103/RevModPhys.70.1039](https://doi.org/10.1103/RevModPhys.70.1039). URL: <https://link.aps.org/doi/10.1103/RevModPhys.70.1039>.

[3] J. E. Hirsch. “Two-dimensional Hubbard model: Numerical simulation study”. In: *Phys. Rev. B* 31 (7 1985), pp. 4403–4419. DOI: [10.1103/PhysRevB.31.4403](https://doi.org/10.1103/PhysRevB.31.4403). URL: <https://link.aps.org/doi/10.1103/PhysRevB.31.4403>.

[4] Leon Balents. “Spin liquids in frustrated magnets”. In: *Nature* 464.7286 (2010), pp. 199–208. DOI: [10.1038/nature08917](https://doi.org/10.1038/nature08917). URL: <https://doi.org/10.1038/nature08917>.

[5] Lucile Savary and Leon Balents. “Quantum spin liquids: a review”. In: *Reports on Progress in Physics* 80.1 (2016), p. 016502. DOI: [10.1088/0034-4885/80/1/016502](https://doi.org/10.1088/0034-4885/80/1/016502). URL: <https://doi.org/10.1088/0034-4885/80/1/016502>.

[6] Yi Zhou, Kazushi Kanoda, and Tai-Kai Ng. “Quantum spin liquid states”. In: *Rev. Mod. Phys.* 89 (2 2017), p. 025003. DOI: [10.1103/RevModPhys.89.025003](https://doi.org/10.1103/RevModPhys.89.025003). URL: <https://link.aps.org/doi/10.1103/RevModPhys.89.025003>.

[7] Chetan Nayak et al. “Non-Abelian anyons and topological quantum computation”. In: *Rev. Mod. Phys.* 80 (3 2008), pp. 1083–1159. DOI: [10.1103/RevModPhys.80.1083](https://doi.org/10.1103/RevModPhys.80.1083). URL: <https://link.aps.org/doi/10.1103/RevModPhys.80.1083>.

[8] P.W. Anderson. “Resonating valence bonds: A new kind of insulator?” In: *Materials Research Bulletin* 8.2 (Feb. 1973), pp. 153–160. DOI: [10.1016/0025-5408\(73\)90167-0](https://doi.org/10.1016/0025-5408(73)90167-0). URL: [https://doi.org/10.1016/0025-5408\(73\)90167-0](https://doi.org/10.1016/0025-5408(73)90167-0).

[9] P. W. Anderson. “The Resonating Valence Bond State in La_2CuO_4 and Superconductivity”. In: *Science* 235.4793 (1987), pp. 1196–1198. ISSN: 0036-8075.

DOI: 10.1126/science.235.4793.1196. eprint: <https://science.sciencemag.org/content/235/4793/1196.full.pdf>. URL: <https://science.sciencemag.org/content/235/4793/1196>.

[10] Y. Shimizu et al. “Spin Liquid State in an Organic Mott Insulator with a Triangular Lattice”. In: *Phys. Rev. Lett.* 91 (10 2003), p. 107001. DOI: 10.1103/PhysRevLett.91.107001. URL: <https://link.aps.org/doi/10.1103/PhysRevLett.91.107001>.

[11] Y. Kuroaki et al. “Mott Transition from a Spin Liquid to a Fermi Liquid in the Spin-Frustrated Organic Conductor κ -(ET)₂Cu₂(CN)₃”. In: *Phys. Rev. Lett.* 95 (17 2005), p. 177001. DOI: 10.1103/PhysRevLett.95.177001. URL: <https://link.aps.org/doi/10.1103/PhysRevLett.95.177001>.

[12] Satoshi Yamashita et al. “Thermodynamic properties of a spin-1/2 spin-liquid state in a κ -type organic salt”. In: *Nature Physics* 4.6 (Apr. 2008), pp. 459–462. DOI: 10.1038/nphys942. URL: <https://doi.org/10.1038/nphys942>.

[13] Takayuki Isono et al. “Gapless Quantum Spin Liquid in an Organic Spin-1/2 Triangular-Lattice κ - H₃(Cat-EDT-TTF)₂”. In: *Phys. Rev. Lett.* 112 (17 2014), p. 177201. DOI: 10.1103/PhysRevLett.112.177201. URL: <https://link.aps.org/doi/10.1103/PhysRevLett.112.177201>.

[14] Björn Miksch et al. “Gapped magnetic ground state in quantum spin liquid candidate κ -(BEDT-TTF)₂Cu₂(CN)₃”. In: *Science* 372.6539 (Apr. 2021), pp. 276–279. DOI: 10.1126/science.abc6363. URL: <https://doi.org/10.1126/science.abc6363>.

[15] Olexei I. Motrunich. “Variational study of triangular lattice spin-1/2 model with ring exchanges and spin liquid state in κ -(ET)₂Cu₂(CN)₃”. In: *Phys. Rev. B* 72 (4 2005), p. 045105. DOI: 10.1103/PhysRevB.72.045105. URL: <https://link.aps.org/doi/10.1103/PhysRevB.72.045105>.

[16] Sung-Sik Lee and Patrick A. Lee. “U(1) Gauge Theory of the Hubbard Model: Spin Liquid States and Possible Application to κ -(BEDT-TTF)₂Cu₂(CN)₃”. In: *Phys. Rev. Lett.* 95 (3 2005), p. 036403. DOI: 10.1103/PhysRevLett.95.036403. URL: <https://link.aps.org/doi/10.1103/PhysRevLett.95.036403>.

[17] Darrell F. Schroeter et al. “Spin Hamiltonian for which the Chiral Spin Liquid is the Exact Ground State”. In: *Phys. Rev. Lett.* 99 (9 2007), p. 097202. DOI: 10.1103/PhysRevLett.99.097202. URL: <https://link.aps.org/doi/10.1103/PhysRevLett.99.097202>.

[18] D. N. Sheng, Olexei I. Motrunich, and Matthew P. A. Fisher. “Spin Bose-metal phase in a spin- $\frac{1}{2}$ model with ring exchange on a two-leg triangular strip”. In: *Phys. Rev. B* 79 (20 2009), p. 205112. DOI: 10.1103/PhysRevB.79.205112. URL: <https://link.aps.org/doi/10.1103/PhysRevB.79.205112>.

[19] Hong-Yu Yang et al. “Effective Spin Model for the Spin-Liquid Phase of the Hubbard Model on the Triangular Lattice”. In: *Phys. Rev. Lett.* 105 (26 2010), p. 267204. DOI: 10.1103/PhysRevLett.105.267204. URL: <https://link.aps.org/doi/10.1103/PhysRevLett.105.267204>.

[20] Tessa Cookmeyer, Johannes Motruk, and Joel E. Moore. “Four-Spin Terms and the Origin of the Chiral Spin Liquid in Mott Insulators on the Triangular Lattice”. In: *Phys. Rev. Lett.* 127 (8 2021), p. 087201. DOI: 10.1103/PhysRevLett.127.087201. URL: <https://link.aps.org/doi/10.1103/PhysRevLett.127.087201>.

[21] Fengcheng Wu et al. “Hubbard Model Physics in Transition Metal Dichalcogenide Moiré Bands”. In: *Phys. Rev. Lett.* 121 (2 2018), p. 026402. DOI: 10.1103/PhysRevLett.121.026402. URL: <https://link.aps.org/doi/10.1103/PhysRevLett.121.026402>.

[22] Yanhao Tang et al. “Simulation of Hubbard model physics in WSe₂/WS₂ moiré superlattices”. In: *Nature* 579.7799 (Mar.

2020), pp. 353–358. DOI: 10.1038/s41586-020-2085-3. URL: <https://doi.org/10.1038/s41586-020-2085-3>.

[23] Jin Yang et al. “Site-Resolved Imaging of Ultracold Fermions in a Triangular-Lattice Quantum Gas Microscope”. In: *PRX Quantum* 2 (2 2021), p. 020344. DOI: 10.1103/PRXQuantum.2.020344. URL: <https://link.aps.org/doi/10.1103/PRXQuantum.2.020344>.

[24] Steven R. White and A. L. Chernyshov. “Neél Order in Square and Triangular Lattice Heisenberg Models”. In: *Phys. Rev. Lett.* 99 (12 2007), p. 127004. DOI: 10.1103/PhysRevLett.99.127004. URL: <https://link.aps.org/doi/10.1103/PhysRevLett.99.127004>.

[25] S. Raghu, S. A. Kivelson, and D. J. Scalapino. “Superconductivity in the repulsive Hubbard model: An asymptotically exact weak-coupling solution”. In: *Phys. Rev. B* 81 (22 2010), p. 224505. DOI: 10.1103/PhysRevB.81.224505. URL: <https://link.aps.org/doi/10.1103/PhysRevB.81.224505>.

[26] Rahul Nandkishore, Ronny Thomale, and Andrey V. Chubukov. “Superconductivity from weak repulsion in hexagonal lattice systems”. In: *Phys. Rev. B* 89 (14 2014), p. 144501. DOI: 10.1103/PhysRevB.89.144501. URL: <https://link.aps.org/doi/10.1103/PhysRevB.89.144501>.

[27] Yuval Gannot, Yi-Fan Jiang, and Steven A. Kivelson. “Hubbard ladders at small U revisited”. In: *Phys. Rev. B* 102 (11 2020), p. 115136. DOI: 10.1103/PhysRevB.102.115136. URL: <https://link.aps.org/doi/10.1103/PhysRevB.102.115136>.

[28] V. Kalmeyer and R. B. Laughlin. “Equivalence of the resonating-valence-bond and fractional quantum Hall states”. In: *Phys. Rev. Lett.* 59 (18 1987), pp. 2095–2098. DOI: 10.1103/PhysRevLett.59.2095. URL: <https://link.aps.org/doi/10.1103/PhysRevLett.59.2095>.

[29] Vadim Kalmeyer and R. B. Laughlin. “Theory of the spin liquid state of the Heisenberg antiferromagnet”. In: *Phys. Rev. B* 39 (16 1989), pp. 11879–11899. DOI: 10.1103/PhysRevB.39.11879. URL: <https://link.aps.org/doi/10.1103/PhysRevB.39.11879>.

[30] X. G. Wen, Frank Wilczek, and A. Zee. “Chiral spin states and superconductivity”. In: *Phys. Rev. B* 39 (16 1989), pp. 11413–11423. DOI: 10.1103/PhysRevB.39.11413. URL: <https://link.aps.org/doi/10.1103/PhysRevB.39.11413>.

[31] Peyman Sahebsara and David Sénéchal. “Hubbard Model on the Triangular Lattice: Spiral Order and Spin Liquid”. In: *Phys. Rev. Lett.* 100 (13 2008), p. 136402. DOI: 10.1103/PhysRevLett.100.136402. URL: <https://link.aps.org/doi/10.1103/PhysRevLett.100.136402>.

[32] A. Yamada. “Magnetic properties and Mott transition in the Hubbard model on the anisotropic triangular lattice”. In: *Phys. Rev. B* 89 (19 2014), p. 195108. DOI: 10.1103/PhysRevB.89.195108. URL: <https://link.aps.org/doi/10.1103/PhysRevB.89.195108>.

[33] Manuel Laubach et al. “Phase diagram of the Hubbard model on the anisotropic triangular lattice”. In: *Phys. Rev. B* 91 (24 2015), p. 245125. DOI: 10.1103/PhysRevB.91.245125. URL: <https://link.aps.org/doi/10.1103/PhysRevB.91.245125>.

[34] Hidekazu Morita, Shinji Watanabe, and Masatoshi Imada. “Nonmagnetic Insulating States near the Mott Transitions on Lattices with Geometrical Frustration and Implications for κ -(ET)₂Cu₂(CN)₃”. In: *Journal of the Physical Society of Japan* 71.9 (Sept. 2002), pp. 2109–2112. DOI: 10.1143/jpsj.71.2109. URL: <https://doi.org/10.1143/jpsj.71.2109>.

[35] Takuya Yoshioka, Akihisa Koga, and Norio Kawakami. “Quantum Phase Transitions in the Hubbard Model on a Triangular Lattice”. In: *Phys. Rev. Lett.* 103 (3 2009), p. 036401. DOI: 10.1103/PhysRevLett.103.036401. URL: <https://link.aps.org/doi/10.1103/PhysRevLett.103.036401>.

aps.org/doi/10.1103/PhysRevLett.103.036401.

[36] A. E. Antipov et al. “Electron energy spectrum of the spin-liquid state in a frustrated Hubbard model”. In: *Phys. Rev. B* 83 (11 2011), p. 115126. DOI: 10.1103/PhysRevB.83.115126. URL: <https://link.aps.org/doi/10.1103/PhysRevB.83.115126>.

[37] Takashi Koretsune, Yukitoshi Motome, and Akira Furusaki. “Exact Diagonalization Study of Mott Transition in the Hubbard Model on an Anisotropic Triangular Lattice”. In: *Journal of the Physical Society of Japan* 76.7 (July 2007), p. 074719. DOI: 10.1143/jpsj.76.074719. URL: <https://doi.org/10.1143/jpsj.76.074719>.

[38] Tomonori Shirakawa et al. “Ground-state phase diagram of the triangular lattice Hubbard model by the density-matrix renormalization group method”. In: *Phys. Rev. B* 96 (20 2017), p. 205130. DOI: 10.1103/PhysRevB.96.205130. URL: <https://link.aps.org/doi/10.1103/PhysRevB.96.205130>.

[39] Aaron Szasz et al. “Chiral Spin Liquid Phase of the Triangular Lattice Hubbard Model: A Density Matrix Renormalization Group Study”. In: *Phys. Rev. X* 10 (2 2020), p. 021042. DOI: 10.1103/PhysRevX.10.021042. URL: <https://link.aps.org/doi/10.1103/PhysRevX.10.021042>.

[40] Aaron Szasz and Johannes Motruk. “Phase diagram of the anisotropic triangular lattice Hubbard model”. In: *Phys. Rev. B* 103 (23 2021), p. 235132. DOI: 10.1103/PhysRevB.103.235132. URL: <https://link.aps.org/doi/10.1103/PhysRevB.103.235132>.

[41] Bin-Bin Chen et al. “Quantum spin liquid with emergent chiral order in the triangular-lattice Hubbard model”. In: *Phys. Rev. B* 106 (9 2022), p. 094420. DOI: 10.1103/PhysRevB.106.094420. URL: <https://link.aps.org/doi/10.1103/PhysRevB.106.094420>.

[42] Luca F. Tocchio, Arianna Montorsi, and Federico Becca. “Magnetic and spin-liquid phases in the frustrated $t - t'$ Hubbard model on the triangular lattice”. In: *Phys. Rev. B* 102 (11 2020), p. 115150. DOI: 10.1103/PhysRevB.102.115150. URL: <https://link.aps.org/doi/10.1103/PhysRevB.102.115150>.

[43] Luca F. Tocchio, Arianna Montorsi, and Federico Becca. “Hubbard model on triangular N -leg cylinders: Chiral and nonchiral spin liquids”. In: *Phys. Rev. Research* 3 (4 2021), p. 043082. DOI: 10.1103/PhysRevResearch.3.043082. URL: <https://link.aps.org/doi/10.1103/PhysRevResearch.3.043082>.

[44] Hunpyo Lee, Gang Li, and Hartmut Monien. “Hubbard model on the triangular lattice using dynamical cluster approximation and dual fermion methods”. In: *Phys. Rev. B* 78 (20 2008), p. 205117. DOI: 10.1103/PhysRevB.78.205117. URL: <https://link.aps.org/doi/10.1103/PhysRevB.78.205117>.

[45] T. Watanabe et al. “Predominant magnetic states in the Hubbard model on anisotropic triangular lattices”. In: *Phys. Rev. B* 77 (21 2008), p. 214505. DOI: 10.1103/PhysRevB.77.214505. URL: <https://link.aps.org/doi/10.1103/PhysRevB.77.214505>.

[46] Luca F. Tocchio et al. “Spin-liquid versus spiral-order phases in the anisotropic triangular lattice”. In: *Phys. Rev. B* 87 (3 2013), p. 035143. DOI: 10.1103/PhysRevB.87.035143. URL: <https://link.aps.org/doi/10.1103/PhysRevB.87.035143>.

[47] Alexander Wietek et al. “Mott Insulating States with Competing Orders in the Triangular Lattice Hubbard Model”. In: *Phys. Rev. X* 11 (4 2021), p. 041013. DOI: 10.1103/PhysRevX.11.041013. URL: <https://link.aps.org/doi/10.1103/PhysRevX.11.041013>.

[48] Patrick A. Lee, Naoto Nagaosa, and Xiao-Gang Wen. “Doping a Mott insulator: Physics of high-temperature superconductivity”. In: *Rev. Mod. Phys.* 78 (1

2006), pp. 17–85. DOI: [10.1103/RevModPhys.78.17](https://doi.org/10.1103/RevModPhys.78.17). URL: <https://link.aps.org/doi/10.1103/RevModPhys.78.17>.

[49] B J Powell and Ross H McKenzie. “Quantum frustration in organic Mott insulators: from spin liquids to unconventional superconductors”. In: *Reports on Progress in Physics* 74.5 (Apr. 2011), p. 056501. DOI: [10.1088/0034-4885/74/5/056501](https://doi.org/10.1088/0034-4885/74/5/056501). URL: <https://doi.org/10.1088/0034-4885/74/5/056501>.

[50] Kazushi Kanoda and Reizo Kato. “Mott Physics in Organic Conductors with Triangular Lattices”. In: *Annual Review of Condensed Matter Physics* 2.1 (Mar. 2011), pp. 167–188. DOI: [10.1146/annurev-conmatphys-062910-140521](https://doi.org/10.1146/annurev-conmatphys-062910-140521). URL: <https://doi.org/10.1146/annurev-conmatphys-062910-140521>.

[51] Annabelle Bohrdt et al. “Exploration of doped quantum magnets with ultracold atoms”. In: *Annals of Physics* 435 (2021). Special issue on Philip W. Anderson, p. 168651. ISSN: 0003-4916. DOI: <https://doi.org/10.1016/j.aop.2021.168651>. URL: <https://www.sciencedirect.com/science/article/pii/S0003491621002578>.

[52] Zheng Zhu, D. N. Sheng, and Ashvin Vishwanath. “Doped Mott insulators in the triangular-lattice Hubbard model”. In: *Phys. Rev. B* 105 (20 2022), p. 205110. DOI: [10.1103/PhysRevB.105.205110](https://doi.org/10.1103/PhysRevB.105.205110). URL: <https://link.aps.org/doi/10.1103/PhysRevB.105.205110>.

[53] Jayadev Vijayan et al. “Time-resolved observation of spin-charge deconfinement in fermionic Hubbard chains”. In: *Science* 367.6474 (Jan. 2020), pp. 186–189. DOI: [10.1126/science.aay2354](https://doi.org/10.1126/science.aay2354). URL: <https://doi.org/10.1126/science.aay2354>.

[54] Wilhelm Kadow, Laurens Vanderstraeten, and Michael Knap. “Hole spectral function of a chiral spin liquid in the triangular lattice Hubbard model”. In: *Phys. Rev. B* 106 (9 2022), p. 094417. DOI: [10.1103/PhysRevB.106.094417](https://doi.org/10.1103/PhysRevB.106.094417). URL: <https://link.aps.org/doi/10.1103/PhysRevB.106.094417>.

[55] Yixuan Huang and D. N. Sheng. “Topological Chiral and Nematic Superconductivity by Doping Mott Insulators on Triangular Lattice”. In: *Phys. Rev. X* 12 (3 2022), p. 031009. DOI: [10.1103/PhysRevX.12.031009](https://doi.org/10.1103/PhysRevX.12.031009). URL: <https://link.aps.org/doi/10.1103/PhysRevX.12.031009>.

[56] Davis Garwood et al. “Site-resolved observables in the doped spin-imbalanced triangular Hubbard model”. In: *Phys. Rev. A* 106 (1 2022), p. 013310. DOI: [10.1103/PhysRevA.106.013310](https://doi.org/10.1103/PhysRevA.106.013310). URL: <https://link.aps.org/doi/10.1103/PhysRevA.106.013310>.

[57] Matthias Troyer and Uwe-Jens Wiese. “Computational Complexity and Fundamental Limitations to Fermionic Quantum Monte Carlo Simulations”. In: *Phys. Rev. Lett.* 94 (17 2005), p. 170201. DOI: [10.1103/PhysRevLett.94.170201](https://doi.org/10.1103/PhysRevLett.94.170201). URL: <https://link.aps.org/doi/10.1103/PhysRevLett.94.170201>.

[58] Shiwei Zhang, J. Carlson, and J. E. Gubernatis. “Constrained Path Quantum Monte Carlo Method for Fermion Ground States”. In: *Phys. Rev. Lett.* 74 (18 1995), pp. 3652–3655. DOI: [10.1103/PhysRevLett.74.3652](https://doi.org/10.1103/PhysRevLett.74.3652). URL: <https://link.aps.org/doi/10.1103/PhysRevLett.74.3652>.

[59] Shiwei Zhang, J. Carlson, and J. E. Gubernatis. “Constrained path Monte Carlo method for fermion ground states”. In: *Phys. Rev. B* 55 (12 1997), pp. 7464–7477. DOI: [10.1103/PhysRevB.55.7464](https://doi.org/10.1103/PhysRevB.55.7464). URL: <https://link.aps.org/doi/10.1103/PhysRevB.55.7464>.

[60] Huy Nguyen et al. “CPMC-Lab: A Matlab package for Constrained Path Monte Carlo calculations”. In: *Computer Physics Communications* 185.12 (2014), pp. 3344–3357. ISSN: 0010-4655. DOI: <https://doi.org/10.1016/j.cpc.2014.08.003>. URL: <https://www.sciencedirect.com/science/article/pii/S0010465514002707>.

[61] J. P. F. LeBlanc et al. “Solutions of the Two-Dimensional Hubbard Model: Benchmarks and Results from a Wide Range of Numerical Algorithms”. In: *Phys. Rev. X*

5 (4 2015), p. 041041. DOI: 10.1103/PhysRevX.5.041041. URL: <https://link.aps.org/doi/10.1103/PhysRevX.5.041041>.

[62] Mingpu Qin, Hao Shi, and Shiwei Zhang. “Benchmark study of the two-dimensional Hubbard model with auxiliary-field quantum Monte Carlo method”. In: *Phys. Rev. B* 94 (8 2016), p. 085103. DOI: 10.1103/PhysRevB.94.085103. URL: <https://link.aps.org/doi/10.1103/PhysRevB.94.085103>.

[63] R. P. Feynman. “Atomic Theory of the Two-Fluid Model of Liquid Helium”. In: *Phys. Rev.* 94 (2 1954), pp. 262–277. DOI: 10.1103/PhysRev.94.262. URL: <https://link.aps.org/doi/10.1103/PhysRev.94.262>.

[64] Manuela Capello et al. “Variational Description of Mott Insulators”. In: *Phys. Rev. Lett.* 94 (2 2005), p. 026406. DOI: 10.1103/PhysRevLett.94.026406. URL: <https://link.aps.org/doi/10.1103/PhysRevLett.94.026406>.

[65] J. Kokalj and Ross H. McKenzie. “Thermodynamics of a Bad Metal–Mott Insulator Transition in the Presence of Frustration”. In: *Phys. Rev. Lett.* 110 (20 2013), p. 206402. DOI: 10.1103/PhysRevLett.110.206402. URL: <https://link.aps.org/doi/10.1103/PhysRevLett.110.206402>.

[66] W. F. Brinkman and T. M. Rice. “Application of Gutzwiller’s Variational Method to the Metal-Insulator Transition”. In: *Phys. Rev. B* 2 (10 1970), pp. 4302–4304. DOI: 10.1103/PhysRevB.2.4302. URL: <https://link.aps.org/doi/10.1103/PhysRevB.2.4302>.

[67] Henk Eskes et al. “Spectral properties of the Hubbard bands”. In: *Phys. Rev. B* 50 (24 1994), pp. 17980–18002. DOI: 10.1103/PhysRevB.50.17980. URL: <https://link.aps.org/doi/10.1103/PhysRevB.50.17980>.

[68] B. Bernu, C. Lhuillier, and L. Pierre. “Signature of Néel order in exact spectra of quantum antiferromagnets on finite lattices”. In: *Phys. Rev. Lett.* 69 (17 1992), pp. 2590–2593. DOI: 10.1103/PhysRevLett.69.2590. URL: <https://link.aps.org/doi/10.1103/PhysRevLett.69.2590>.

[69] Christie S. Chiu et al. “String patterns in the doped Hubbard model”. In: *Science* 365.6450 (July 2019), pp. 251–256. DOI: 10.1126/science.aav3587. URL: <https://doi.org/10.1126/science.aav3587>.

[70] Konrad Viebahn et al. “Matter-Wave Diffraction from a Quasicrystalline Optical Lattice”. In: *Phys. Rev. Lett.* 122 (11 2019), p. 110404. DOI: 10.1103/PhysRevLett.122.110404. URL: <https://link.aps.org/doi/10.1103/PhysRevLett.122.110404>.

[71] Matteo Sbroscia et al. “Observing Localization in a 2D Quasicrystalline Optical Lattice”. In: *Phys. Rev. Lett.* 125 (20 2020), p. 200604. DOI: 10.1103/PhysRevLett.125.200604. URL: <https://link.aps.org/doi/10.1103/PhysRevLett.125.200604>.

[72] A. Mendoza-Coto et al. “Exploring quantum quasicrystal patterns: A variational study”. In: *Phys. Rev. B* 105 (13 2022), p. 134521. DOI: 10.1103/PhysRevB.105.134521. URL: <https://link.aps.org/doi/10.1103/PhysRevB.105.134521>.

[73] Ronan Gautier, Hepeng Yao, and Laurent Sanchez-Palencia. “Strongly Interacting Bosons in a Two-Dimensional Quasicrystal Lattice”. In: *Phys. Rev. Lett.* 126 (11 2021), p. 110401. DOI: 10.1103/PhysRevLett.126.110401. URL: <https://link.aps.org/doi/10.1103/PhysRevLett.126.110401>.

[74] Matteo Ciardi, Tommaso Macrì, and Fabio Cinti. “Finite-temperature phases of trapped bosons in a two-dimensional quasiperiodic potential”. In: *Phys. Rev. A* 105 (1 2022), p. L011301. DOI: 10.1103/PhysRevA.105.L011301. URL: <https://link.aps.org/doi/10.1103/PhysRevA.105.L011301>.

[75] T. Macrì and T. Pohl. “Rydberg dressing of atoms in optical lattices”. In: *Phys. Rev. A* 89 (1 2014), p. 011402. DOI: 10.1103/PhysRevA.89.011402. URL: <https://link.aps.org/doi/10.1103/PhysRevA.89.011402>.

[76] Peter Schauss. “Quantum simulation of transverse Ising models with Rydberg atoms”. In: *Quantum Science and Technology* 3.2 (2018), p. 023001. DOI: 10.1088/2058-9565/aa9c59. URL: <https://doi.org/10.1088/2058-9565/aa9c59>.

[77] Nicolò Defenu et al. *Long-range interacting quantum systems*. 2021. DOI: 10.48550/ARXIV.2109.01063. URL: <https://arxiv.org/abs/2109.01063>.

[78] Elmer Guardado-Sánchez et al. “Quench Dynamics of a Fermi Gas with Strong Non-local Interactions”. In: *Phys. Rev. X* 11 (2 2021), p. 021036. DOI: 10.1103/PhysRevX.11.021036. URL: <https://link.aps.org/doi/10.1103/PhysRevX.11.021036>.

[79] V. Zampronio. *CP-AFQMC*. 2022. URL: <https://github.com/quantechsimulation/CP-AFQMC>.

[80] H. F. Trotter. “On the product of semi-groups of operators”. In: *Proc. Amer. Math. Soc.* 10 (1959), pp. 545–551. DOI: <https://doi.org/10.1090/S0002-9939-1959-0108732-6>. URL: <https://www.ams.org/journals/proc/1959-010-04/S0002-9939-1959-0108732-6/home.html#Additional>.

[81] Peter J. Reynolds et al. “Fixed-node quantum Monte Carlo for molecules a)-b)”. In: *The Journal of Chemical Physics* 77.11 (1982), pp. 5593–5603. DOI: 10.1063/1.443766. eprint: <https://doi.org/10.1063/1.443766>. URL: <https://doi.org/10.1063/1.443766>.

[82] X. Y. Zhang, Elihu Abrahams, and G. Kotliar. “Quantum Monte Carlo algorithm for constrained fermions: Application to the infinite-U Hubbard model”. In: *Phys. Rev. Lett.* 66 (9 1991), pp. 1236–1239. DOI: 10.1103/PhysRevLett.66.1236. URL: <https://link.aps.org/doi/10.1103/PhysRevLett.66.1236>.

[83] Wirawan Purwanto and Shiwei Zhang. “Quantum Monte Carlo method for the ground state of many-boson systems”. In: *Phys. Rev. E* 70 (5 2004), p. 056702. DOI: 10.1103/PhysRevE.70.056702. URL: <https://link.aps.org/doi/10.1103/PhysRevE.70.056702>.

A Constrained path AFQMC

Let a given initial state $|\Psi(0)\rangle$ be nonorthogonal to the ground-state of the Hamiltonian H , $|\Psi_0\rangle$. The imaginary-time evolution $|\Psi(\tau)\rangle = \exp(-\tau H)|\Psi(0)\rangle$ will asymptotically converge to $|\Psi_0\rangle$ as τ (a real number) increases. In the AFQMC method the anti-symmetric wave function is written as a linear combination of Slater determinants

$$|\Psi(\tau)\rangle = \sum_k \xi(\Phi_k) |\Phi_k(\tau)\rangle. \quad (7)$$

In our simulations, $\xi(\Phi_k)$ is not considered explicitly. As the imaginary-time evolution proceeds, Slater determinants are replicated or killed. The number of a given $|\Phi_k\rangle$ in the sum resembles $\xi(\Phi_k)$ [58, 59]. In practice one starts at $\tau = 0$ with all Slater Determinants equal to a given trial state $|\Phi_T\rangle$, an approximation to the ground state usually obtained from mean-field theories, and update them by the application of the imaginary-time evolution operator in a stochastic process. For large systems the diagonalization of the FH Hamiltonian becomes impractical. It is then usual to consider the Trotter formula [80] to factor the evolution operator into the product of three therm

$$e^{-\delta\tau H} = e^{-\frac{\delta\tau}{2}K} e^{-\delta\tau V} e^{-\frac{\delta\tau}{2}K} + \mathcal{O}(\delta\tau^2), \quad (8)$$

where, for the Fermi Hubbard (FH) Hamiltonian, K (V) is the hopping (interaction) therm. If we chose $\delta\tau$ small enough, the error introduced by neglecting the $\mathcal{O}(\delta\tau^2)$ therm in Eq. (8) can be made smaller than the statistical uncertainty inherent to Monte Carlo calculations; the method remains numerically exact. The desired limit $\tau = n\delta\tau \gg t^{-1}$, with t being the hopping strength, is obtained after n successive applications of this small- $\delta\tau$ approximation to $|\Psi(0)\rangle$. A given iteration on the Slater Determinants is

$$|\Phi_k^{n+1}\rangle = e^{-\frac{\delta\tau}{2}K} e^{-\delta\tau V} e^{-\frac{\delta\tau}{2}K} |\Phi_k^n\rangle, \quad (9)$$

where the superscript n indicates the imaginary time $\tau = n\delta\tau$. The application of one-body operators in $|\Phi_k^n\rangle$ results in another Slater Determinant. Therefore, both $\exp(-\delta\tau K/2)$ only propagates $|\Phi_k^n\rangle$. On the other hand, since V is a sum of two-body operators, the remaining exponential imposes a challenge. To handle it, one can use the Hubbard-Stratonovich decomposition to transform the two-body interaction into one-body ones between each electron and auxiliary fields x . We choose the spin discrete decomposition [3],

$$e^{-\delta\tau n_{i\uparrow} n_{i\downarrow}} = e^{-\frac{\delta\tau}{2}U(n_{i\uparrow} + n_{i\downarrow})} \sum_{x=\pm 1} p(x) e^{\gamma x(n_{i\uparrow} - n_{i\downarrow})}, \quad (10)$$

with $p(x) = 1/2$ and γ being given by the relation $\cosh(\gamma) = \exp(\delta\tau U/2)$. Considering the FH Hamiltonian H , one writes

$$e^{\delta\tau H} \approx \sum_{\vec{x}} p(\vec{x}) e^{-\frac{\beta}{2}K} B_V(\vec{x}) e^{-\frac{\beta}{2}K}, \quad (11)$$

where $\vec{x} = (x_1, x_2, \dots, x_M)$ is a configuration of auxiliary fields, with M the number of lattice sites, to be sampled within Monte Carlo calculations, $p(\vec{x}) = (1/2)^M$ is a probability distribution function (pdf) and $B_V(\vec{x})$ is a product of one-body exponentials. Explicitly,

$$B_V(\vec{x}) = \prod_i e^{-\frac{\delta\tau}{2}U(n_{i\uparrow} + n_{i\downarrow}) + \gamma x_i(n_{i\uparrow} - n_{i\downarrow})}. \quad (12)$$

The stochastic simulation of Eq. (9) is very inefficient since $p(\vec{x})$ is constant and an importance sampling technique is required [58, 59]. The importance sampling is also useful to define an estimator to the properties of the system and to determine the constraints that eliminate the sign problem. The importance function we implement is $O_T(\Phi_k^n) = \langle \Phi_T | \Phi_k^n \rangle$, which leads to the modified imaginary-time evolution

$$|\tilde{\Psi}^{n+1}\rangle = \sum_{\vec{x}} \tilde{p}(\vec{x}) e^{-\frac{\delta\tau}{2}K} B_V(\vec{x}) e^{-\frac{\delta\tau}{2}K} |\tilde{\Psi}^n\rangle, \quad (13)$$

with the modified pdf $\tilde{p}(\vec{x}) = O_T(\Phi_j^n)p(\vec{x})/O_T(\Phi_j^{n-1})$. The pdf now depends on the overlap with the approximated ground state after and before the diffusion procedure. Since the pdf $\tilde{p}(\vec{x})$ is usually not normalized, we define the normalization factor of each Slater determinant $N(\Phi_k^n)$, and the iterative projection equation becomes

$$|\Phi_k^n\rangle = N(\Phi_k^n) \sum_{\vec{x}} \frac{\tilde{p}(\vec{x})}{N(\Phi_k^n)} e^{-\frac{\delta\tau}{2}K} B_V e^{-\frac{\delta\tau}{2}K} |\Phi_k^{n-1}\rangle. \quad (14)$$

To handle the normalization we introduce weights to each Slater Determinant $|\tilde{\Psi}^n\rangle = \sum_k \omega_k^n |\Phi_k^n\rangle$, and in each iteration the weights are updated as $\omega_k^n = N(\Phi_k^n)\omega_k^{n-1}$, with $\omega_k^0 = 1$. In practice, the sampling of the pdf $\tilde{p}(\vec{x})$ is done considering individually each auxiliary field in the configuration \vec{x} . A detailed description of how to implement the aforementioned sampling and how to updated the weights is given in Ref. [60].

The equivalence between $|\Phi_k^n\rangle = -|\Phi_k^n\rangle$ causes a sign problem that prevents numerical convergence. To eliminate the sign problem, auxiliary-field paths are constrained to a region of the configuration space were $O_T(\Phi_k^n) > 0$ (akin to the fixed-node approximation [81]). Due to the equivalence between the positive and negative regions of the ground state, the method is numerically exact if the nodal structure of the trial wave function is equivalent to the ground-state one. Unfortunately the latter is unknown in the majority of cases and $|\Phi_T\rangle$ carries an approximation to it. For that reason the constrained-path approximation, has a systematic error, which is, however, small [58, 59, 60, 62].

Ground-state estimates of the system total energy can be obtained using the mixed estimator,

$$\langle H \rangle_{\text{mix}} = \frac{\sum_k \omega_k^n E_k^n}{\sum_j \omega_k^n}, \quad (15)$$

with $E_k^n = \langle \Phi_T | H | \Phi_k^n \rangle / O_T(\Phi_k^n)$ and sufficiently large n . As can be noticed, the mixed estimator is only exact if the operator in the numerator of Eq. (15) commutes with the Hamiltonian H .

Estimates of other physical observables require the back-propagation technique [58, 82, 83]. The back-propagation estimator is constructed from the formula

$$\langle O \rangle_{\text{bp}} \propto \langle \Phi_T | e^{-\tau_{\text{bp}} H} O e^{-(\tau - \tau_{\text{bp}}) H} | \Psi(0) \rangle, \quad (16)$$

which asymptotically reaches the average value of the observable O in the ground state for $\tau - \tau_{\text{bp}}$ and $\tau_{\text{bp}} \gg t^{-1}$. The numerical evaluation of Eq. (16) is implemented efficiently by storing the auxiliary fields sampled in the forward propagation $\exp(-\tau_{\text{bp}} H) |\Psi(0)\rangle$ and using them to back propagate $\langle \Phi_T |$. For a detailed description of this estimator see Ref. [83].

Additional simulation details. Our time step is $\delta\tau = 10^{-2}/t$, with 10^3 Slater determinants. Also, we see convergence of our estimates with $\tau_{\text{bp}} = 1.6/t$.

B Finite system size effects

We compute the total energy of the system at half filling for two lattice sizes, with 108 sites ($N_x \times N_y = 9 \times 12$) and 144 sites ($N_x \times N_y = 12 \times 12$). The energies are shown in FIG. 7. Since the energies do not change much we conclude that our results are relatively free from size effects ¹.

C Comparison between 2D and quasi-1D

In FIG. 8 we compare results for S_{max} and χ in 2D (12×12) and quasi-1D (36×3). We see that, for the quasi-1D system, S_{max} suddenly increases for interactions between $11 < U/t \leq 12$ indicating the transition to the AFM phase, while it remains almost constant in the 2D system.

¹In the transition to the magnetic phase there maybe some effects of the system size.

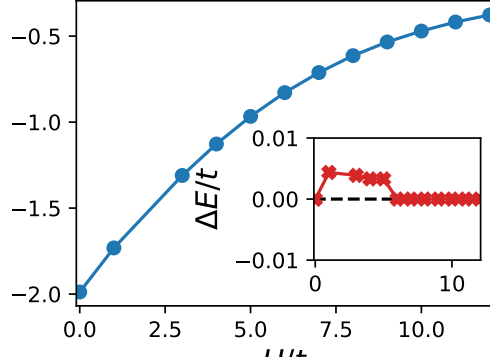


Figure 7: **Total energy per lattice site.** The blue circles represent the 12×12 lattice. In the inset we show the difference ΔE between this energies and the ones obtained in a 9×12 lattice.

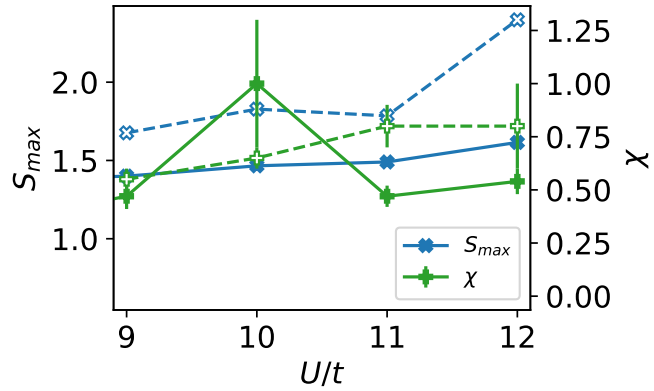


Figure 8: (Color online) **Magnetic versus chiral orders at half filling.** Comparison between results for the 2D lattice (12×12) and the quasi-1D (36×3) one as function of U/t . Filled (empty) markers are results for the 2D (quasi-1D) lattice.

We also compute the Cooper pair correlations for the quasi-1D system at $U/t = 9$, and as expected by the Mermin-Wagner theorem, they do not display long-range order. We considered the fillings $n = 17/18$ and $n = 5/6$, see FIG. 9.

Furthermore, In FIG. 10 we show the spin structure $S(k)$ factor for $U/t = 9, 10, 11$ and 12 . The maxima of $S(k)$ is around $k = K$ for the 2D lattice, but it moves to the $k = M$ in quasi-1D. In the latter case one can see the formation of peaks indicating long-range spin order. In FIG. 10 (c) we show that in the 2D system $S(0)$ assumes a finite value. It happens only for one of the considered interaction in each of our 2D systems: $U/t = 12$ for the 12×12 lattice and $U/t = 10$ for the 9×12 one. This indicates that our simulations provides a finite value to $\sum_{ij} \langle S_i^z S_j^z \rangle$ in this situations. For the quasi-1D system this value is always zero.

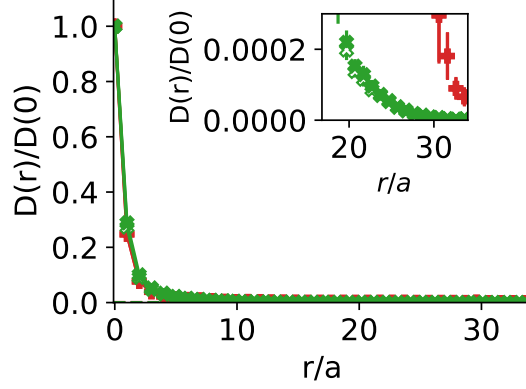


Figure 9: (Color online) **Cooper pair correlations.** Results for the quasi-1D (36×3) lattice. Green 'x' markers represent the results at $n = 5/6$, and red '+' markers are results at $n = 17/18$. Filled symbols are for triplet pairs, and empty ones for singlets (they are degenerate). The inset shows the long-range behavior. The interaction is $U/t = 9$.

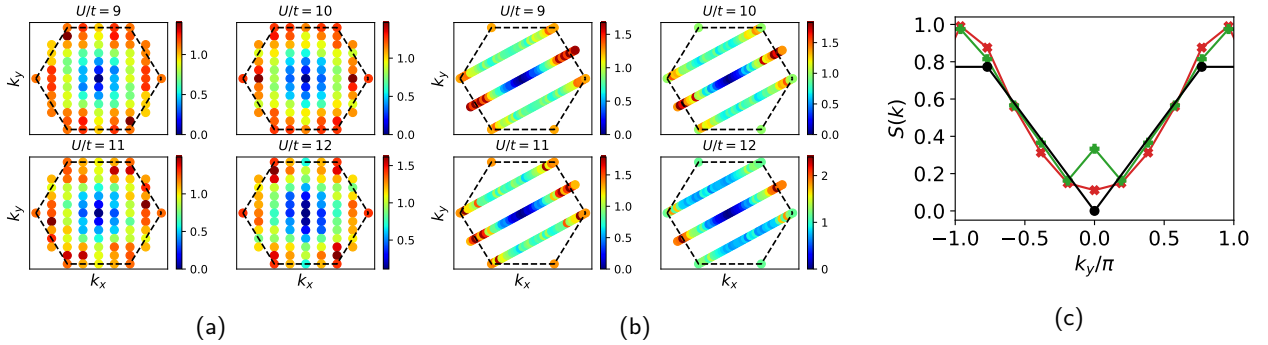


Figure 10: **Spin structure factor** for interactions $U/t = 9, 10, 11$ and 12 at half filling. (a) Results for the 2D lattice with 144 sites. (b) Results for the quasi-1D system with 108 sites. (c) Behavior of $S(k)$ around the origin. The 'x' markers represent the 12×12 system at $U/t = 12$, the '+' ones represent results for the 9×12 lattice at $U/t = 10$. The circles represent the 36×3 lattice at $U/t = 12$. All results are for allowed momenta in the considered geometry.